

Oxygen Reduction to Water Mediated by a Dirhodium Hydrido-Chloride Complex

Thomas S. Teets, Timothy R. Cook, Brian D. McCarthy, and Daniel G. Nocera*

Department of Chemistry, 6-335, Massachusetts Institute of Technology, 77 Massachusetts Avenue, Cambridge, Massachusetts 02139-4307, United States

S Supporting Information

ABSTRACT: The two-electron mixed-valence dirhodium complex $\text{Rh}_2^{0,\text{II}}(\text{tfepma})_2(\text{CN}^t\text{Bu})_2\text{Cl}_2$ ($\text{tfepma} = \text{CH}_3\text{N}[\text{P}(\text{OCH}_2\text{CF}_3)_2]_2$) reacts with HCl to furnish two isomeric dirhodium hydrido-chloride complexes, $\text{Rh}_2^{\text{II,II}}(\text{tfepma})_2(\text{CN}^t\text{Bu})_2\text{Cl}_3\text{H}$. In the presence of HCl , the hydride complex effects the reduction of 0.5 equiv of O_2 to 1 equiv of H_2O , generating $\text{Rh}_2^{\text{II,II}}(\text{tfepma})_2(\text{CN}^t\text{Bu})_2\text{Cl}_4$, which can be prepared independently by chlorine oxidation of the $\text{Rh}_2^{0,\text{II}}$ precursor. The starting $\text{Rh}_2^{0,\text{II}}$ complex is regenerated photochemically to close an oxygen-to-water reduction photocycle.

Multielectron chemistry is supported by metal–metal bonded complexes that feature a stable two-electron mixed-valence oxidation state.¹ Whereas a hydrogen chemistry^{2–5} and associated halogen elimination chemistry^{6–9} have been elaborated for the two-electron mixed valence cores, an oxygen activation chemistry is heretofore unknown. We now report a novel two-electron mixed-valence dirhodium complex, $\text{Rh}_2^{0,\text{II}}(\text{tfepma})_2(\text{CN}^t\text{Bu})_2\text{Cl}_2$ (**1**) ($\text{tfepma} = \text{CH}_3\text{N}[\text{P}(\text{OCH}_2\text{CF}_3)_2]_2$), which reacts with HCl to furnish two hydride isomers of $\text{Rh}_2^{\text{II,II}}(\text{tfepma})_2(\text{CN}^t\text{Bu})_2\text{Cl}_3\text{H}$ (**3a** and **3b**). The hydride is capable of promoting the reduction of molecular oxygen, generating 1 equiv of water per bimetallic complex. The metal-containing product of this transformation is $\text{Rh}_2^{\text{II,II}}(\text{tfepma})_2(\text{CN}^t\text{Bu})_2\text{Cl}_4$ (**2**). We show that this $\text{Rh}_2^{\text{II,II}}\text{Cl}_4$ complex can be photoconverted back to $\text{Rh}_2^{0,\text{II}}$ complex **1**, thereby rendering an oxygen-to-water photocycle.

Two-electron mixed-valence complex **1** is formed in high yields by room temperature reaction of $[\text{Rh}^{\text{I}}(\text{COD})\text{Cl}]_2$ ($\text{COD} = 1,5\text{-cyclooctadiene}$) with 2 equiv of tfepma and CN^tBu . The $^{31}\text{P}\{^1\text{H}\}$ NMR spectrum (20 °C, CD_2Cl_2) shows two distinct signals at 124.5 and 145.1 ppm (Figures S1 and S14), indicative of the coordination asymmetry as a result of the two-electron mixed-valence core. Furthermore, the two closely spaced $\text{C}\equiv\text{NC}(\text{CH}_3)_3$ resonances in the ^1H NMR (Figure S2) and two distinct $\text{C}\equiv\text{N}$ stretching frequencies in the IR (2122 and 2143 cm^{-1}) are also consistent with the assignment of a two-electron mixed-valence core. These spectral conclusions are verified by the X-ray crystal structure of **1**, which is shown in Figure 1. The respective square planar and octahedral environments of the Rh^0 and Rh^{II} centers are evident; the $\text{Rh}(1)\text{--Rh}(2)$ internuclear distance of 2.6807(3) Å indicates a formal metal–metal bond.

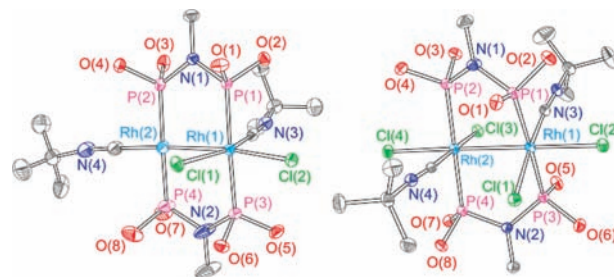


Figure 1. Thermal ellipsoid plots of **1** (left) and **2** (right) drawn at the 50% probability level. The $-\text{CH}_2\text{CF}_3$ groups and hydrogen atoms are omitted for clarity. The $\text{Rh}(1)\text{--Rh}(2)$ distances are 2.6807(3) Å (**1**) and 2.7391(3) Å (**2**).

Treatment of $\text{Rh}_2^{0,\text{II}}$ complex **1** with PhICl_2 in toluene results in a two-electron oxidation to furnish $\text{Rh}_2^{\text{II,II}}$ complex **2**. The asymmetric $^{31}\text{P}\{^1\text{H}\}$ NMR spectrum of **1** collapses to a single symmetric multiplet in **2**, located at 113.8 ppm (Figures S3 and S15). In addition, the ^1H NMR spectrum (Figure S4) and the single $\text{C}\equiv\text{N}$ stretch in the IR (2200 cm^{-1}) are indicative of oxidation of the complex to a valence-symmetric species. The crystal structure shown in Figure 1 confirms the spectral findings of a bimetallic core that possesses pseudo- C_{2h} symmetry. The $\text{Rh}(1)\text{--Rh}(2)$ distance of 2.7391(3) Å establishes that the rhodium–rhodium bond is maintained.

Previous examples of two-electron mixed-valence dirhodium complexes all featured Rh^0 centers that were five-coordinate,¹ and as such, reactivity with acids was not directly observed. In contrast, the Rh^0 center in **1** is four-coordinate, which allows for ground-state addition reactions. Treatment of **1** with HCl results in an equilibrium between two isomeric hydride-containing products and **1**. With a single equivalent of HCl , only ~60% conversion is observed. By using an excess of HCl (25 equiv), near quantitative conversion to $\text{Rh}_2^{\text{II,II}}(\text{tfepma})_2(\text{CN}^t\text{Bu})_2\text{Cl}_3\text{H}$ (**3a** and **3b**) results. The $^{31}\text{P}\{^1\text{H}\}$ and partial ^1H NMR spectra of the reaction products are shown in Figure 2. Integration of the ^1H NMR spectrum reveals that the major isomer, **3a**, is formed in 84% yield along with 14% of **3b** and ~2% of unreacted **1**. The downfield region of the ^1H spectrum shows that each isomer contains two chemically inequivalent CN^tBu resonances (Figure S5). The $\text{Rh}\text{--H}$ resonances shown in Figure 2 appear as doublets of triplets, arising from coupling to two phosphorus atoms and the 100% abundant $I = 1/2$ ^{103}Rh nucleus.

Received: March 3, 2011

Published: May 03, 2011

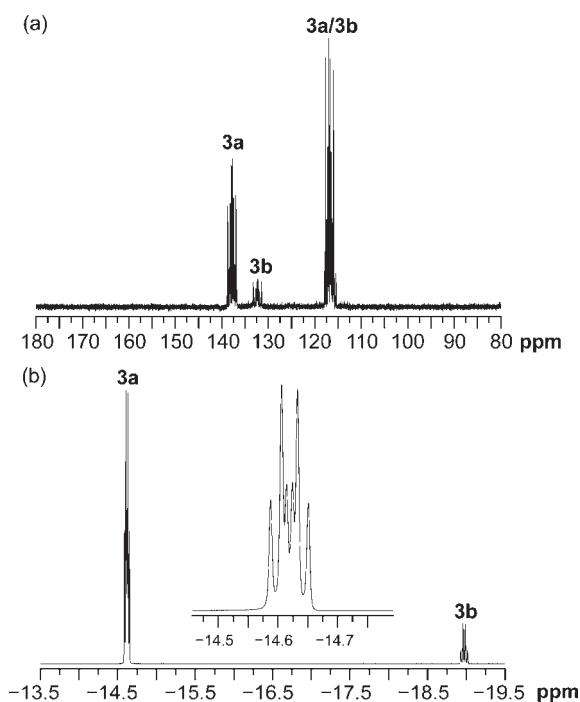


Figure 2. (a) $^{31}\text{P}\{^1\text{H}\}$ and (b) low-frequency ^1H NMR spectra of **3a** and **3b**, prepared by treating **1** with 25 equiv of HCl gas in THF- d_8 . The inset in (b) is an expansion of the Rh–H resonance of **3a**. Spectra were recorded at 20 °C at 202.5 MHz (^{31}P) and 500 MHz (^1H).

The $^1J_{\text{Rh-P}}$ values are 13.3 Hz in **3a** and 14.5 Hz in **3b**, whereas $^2J_{\text{P-H}}$ coupling constants are 9.1 Hz in **3a** and 14.5 Hz in **3b**. By virtue of the equal $^1J_{\text{Rh-P}}$ and $^2J_{\text{P-H}}$ values, the hydride resonance for **3b** appears as a quartet. The observed splitting patterns with relatively small $^2J_{\text{P-H}}$ values indicate that the hydride ligand in both isomers is cis to two equivalent phosphorus nuclei.¹⁰ When a solution of **3a** and **3b** is concentrated to dryness and then redissolved, the $^{31}\text{P}\{^1\text{H}\}$ NMR spectrum shows a mixture of both isomers of **3** and $\text{Rh}_2^{\text{O,II}}$ complex **1** (ca. 40%), confirming the reversible nature of HCl addition to **1**. This ratio is identical to that obtained when **1** is treated with 1 equiv of HCl. Treatment of **1** with excess DCl cleanly furnishes two isomers of $\text{Rh}_2(\text{tfepma})_2(\text{CN}^t\text{Bu})_2\text{Cl}_3\text{D}$, **4a** and **4b**. The NMR spectra (Figures S6 and S7) suggest that **4a** and **4b** are structurally analogous to their hydride analogs and formed in the same ratio.

One of the two isomers of **3** was crystallized; its structure is depicted in Figure 3. Two octahedral Rh^{II} centers are evident, and the Rh(1)–Rh(2) distance of 2.7560(2) Å is once again consistent with a single bond. The hydride ligand is situated trans to a chloride and syn with respect to the chloride on the opposite rhodium center. The second isomer of **3** was not crystallographically characterized, but the NMR data (*vide infra*) are consistent with an analogous structure where the hydride and chloride on Rh(2) exchanged with one another, though any structure featuring a hydride cis to both geminal phosphorus atoms is possible.

Degassed solutions of hydride species **3a** and **3b** display indefinite thermal stability in the presence of excess HCl. However, when a solution of **1** is treated with excess HCl to furnish the hydride and O_2 is subsequently introduced, clean conversion to

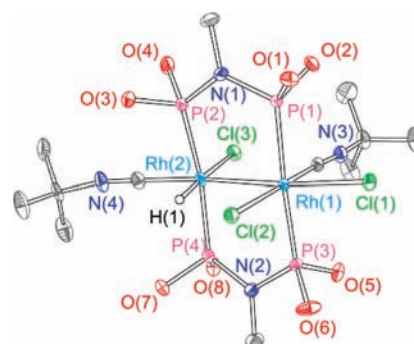
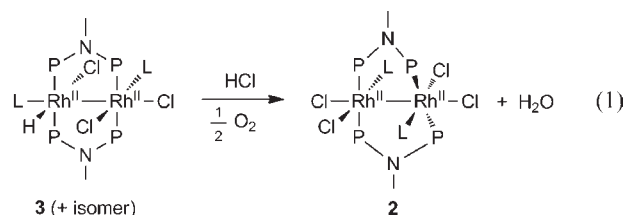


Figure 3. Thermal ellipsoid plot of one of the isomers of **3** drawn at the 50% probability level. The hexane solvate molecule, carbon-bound hydrogen atoms, and $-\text{CH}_2\text{CF}_3$ groups are omitted for clarity. The Rh(1)–Rh(2) distance is 2.7560(2) Å.

$\text{Rh}_2^{\text{II,II}}\text{Cl}_4$ complex **2** is observed over the course of a few hours; the reaction sequence is



Both $^{31}\text{P}\{^1\text{H}\}$ and ^1H NMR spectra attest to the near quantitative yield of **2** (Figures S8 and S9). Inspection of the $^{31}\text{P}\{^1\text{H}\}$ NMR spectrum at intermediate time points shows only **3a**, **3b**, and **2** in solution, with no detectable intermediates on the NMR time scale.

Analogous reactivity is observed for the deuteride complexes **4a** and **4b**. Treatment with O_2 in THF results in quantitative formation of **2** on a comparable time scale, as confirmed by $^{31}\text{P}\{^1\text{H}\}$ NMR (Figure S10). Following neutralization of the unreacted DCl with 2,6-lutidine, which precipitates the deuteriochloride salt, the ^2H NMR spectrum clearly shows the formation of 1 equiv of D_2O , as determined by integration of the broad D_2O resonance (2.7 ppm) against an internal standard of C_6D_6 . A control experiment, treated in an identical fashion but without **1** present at the start, showed negligible amounts of D_2O in the ^2H spectrum. These results confirm that **3** promotes the four-electron, four-proton reduction of O_2 yielding 1 equiv of water per equiv of **3**.

Although no intermediates were detected by NMR, the pathway for reaction 1 likely involves initial formation of a hydroperoxide complex by insertion of O_2 into the Rh–H bond. Studied primarily in the context of aerobic hydrocarbon oxidation, insertion of O_2 into late transition metal hydrides, or alternatively protonation of metal-peroxide complexes, has been shown to furnish stable hydroperoxide complexes, which can be characterized spectroscopically^{11,12} and in some cases crystallographically.^{13–19} To our knowledge, none of these previous examples have been demonstrated to undergo further productive chemistry that results in formation of water. Late metal hydroperoxides have also been invoked as intermediates in O_2 hydrogenation reactions,²⁰ and it is not uncommon to observe evolution to the corresponding metal-hydroxide complex.^{11,14,15,20,21} A rhodium-hydroxide may be the final intermediate prior to water liberation, though at this time we cannot rule out alternative mechanisms, such as the liberation of H_2O_2 followed by dismutation

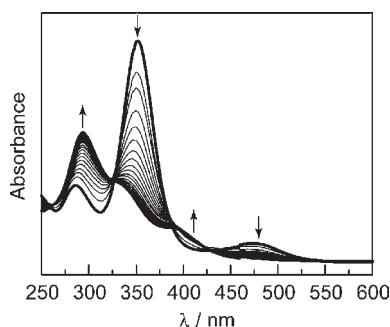
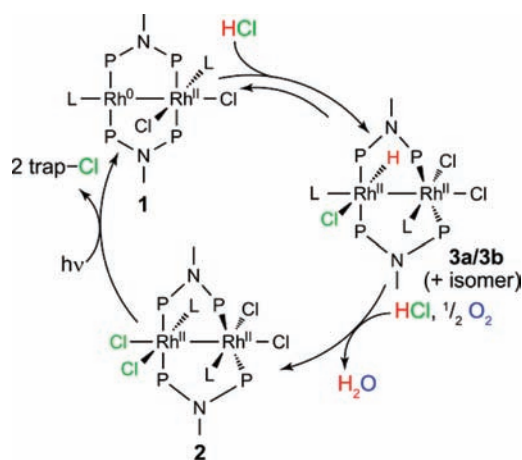


Figure 4. Spectral evolution for the photolysis of **2** ($56 \mu\text{M}$) in THF, using broad-band light with $\lambda > 313 \text{ nm}$. Spectra were recorded every 2 min for a total of 40 min.

Scheme 1



to H_2O and O_2 . That said, it should be noted that ^1H and ^2H NMR spectra of reaction mixtures resulting from treatment of **1** with O_2 and HCl or DCl did not show any evidence for the formation of H_2O_2 . H_2O was the exclusive oxygen-containing product detected by NMR.

The $\text{Rh}_2^{\text{II,II}}$ product **2** generated in reaction 1 can be converted back to **1** photolytically. The UV–vis spectral features of **1** and **2** (Figure S13) are similar to those of other metal–metal bonded late transition metal complexes^{6,22,23} and can be attributed to states arising from the promotion of electrons into the $d\sigma^*$ LUMO. Irradiation of **2** ($\lambda_{\text{exc}} > 313 \text{ nm}$) in THF begets smooth conversion to $\text{Rh}_2^{0,\text{II}}$ complex **1**, which is stable under these photochemical conditions. The UV–vis spectral evolution of the photolysis, shown in Figure 4, clearly indicates the formation of complex **1**. Isosbestic points at 261, 325, 391, and 431 nm attest to the quantitative photoconversion, and the final spectrum is identical to that of an authentic sample of **1**. The product-formation quantum yield, Φ_{p} , was found to be 0.0063(**2**) at $\lambda_{\text{exc}} = 320 \text{ nm}$. This value for Cl photoelimination is somewhat lower than that observed for d^7 – d^7 dirhodium complexes bridged by three dfpma ligands,²⁴ which have quantum yields of 0.05(**1**) when irradiated at 334 nm.

By photochemically regenerating **1** from **2**, the synthetic photocycle shown in Scheme 1 is established. The cycle in Scheme 1 must be carried out in a stepwise fashion owing to the photochemical instability of hydride complexes **3a** and **3b**, as well as deleterious side reactions when **2** is photolyzed in the

presence of oxygen and water, which builds in concentration over the course of the reaction.

To summarize, $\text{Rh}_2^{0,\text{II}}$ complex **1** reacts with HCl in an equilibrium fashion to furnish isomeric hydrido-chloride complexes **3a** and **3b**. The coordinative unsaturation of the Rh^0 center in **1** facilitates the thermal oxidative addition of HCl . The hydride complexes are resistant to protonolysis by additional HCl but react smoothly with O_2 and HCl to furnish $\text{Rh}_2^{\text{II,II}}\text{Cl}_4$ complex **2**, with concomitant generation of H_2O . By using deuterated analogs, the production of 1 equiv of water is confirmed. Product **2** can be photolytically converted back to **1** to complete a catalytic cycle, provided that the excess reactants (HCl and O_2) and the product water are first removed. The sequence shown in Scheme 1 provides an unprecedented example of oxygen reduction facilitated by a two-electron mixed-valence complex. The molecular nature of this transformation permits the clear definition of reaction steps and intermediates, and mechanistic studies to elucidate these details are underway. The multielectron activity observed here expands the utility of the two-electron mixed valence complexes beyond HX splitting. As we continue to explore the reactivity of mixed-valence complexes, we are actively pursuing other demanding small-molecule activation reactions that can be executed on such platforms.

■ ASSOCIATED CONTENT

S Supporting Information. Full details of experimental procedures, NMR spectra for complexes **1**–**4**, NMR spectra for O_2 reduction reactions, UV–vis spectrum of **3a/3b**, simulated $^{31}\text{P}\{^1\text{H}\}$ NMR spectra for **1**–**4**, and crystallographic summary. This material is available free of charge via the Internet at <http://pubs.acs.org>.

■ AUTHOR INFORMATION

Corresponding Author

nocera@mit.edu

■ ACKNOWLEDGMENT

Research was supported by NSF Grant CHE-0750239. Grants from the NSF (CHE-9808061 and DBI-9729592) support the Department of Chemistry Instrumentation Facility. T.S.T. acknowledges the Fannie and John Hertz Foundation for a graduate research fellowship.

■ REFERENCES

- (1) Nocera, D. G. *Inorg. Chem.* **2009**, *48*, 10001.
- (2) Heyduk, A. F.; Nocera, D. G. *Science* **2001**, *293*, 1639.
- (3) Esswein, A. J.; Veige, A. S.; Nocera, D. G. *J. Am. Chem. Soc.* **2005**, *127*, 16641.
- (4) Veige, A. S.; Gray, T. G.; Nocera, D. G. *Inorg. Chem.* **2005**, *44*, 17.
- (5) Gray, T. G.; Veige, A. S.; Nocera, D. G. *J. Am. Chem. Soc.* **2004**, *126*, 9760.
- (6) Cook, T. R.; Surendranath, Y.; Nocera, D. G. *J. Am. Chem. Soc.* **2009**, *131*, 28.
- (7) Teets, T. S.; Neumann, M. P.; Nocera, D. G. *Chem. Commun.* **2011**, *47*, 1485.
- (8) Teets, T. S.; Nocera, D. G. *J. Am. Chem. Soc.* **2009**, *131*, 7411.
- (9) Cook, T. R.; Esswein, A. J.; Nocera, D. G. *J. Am. Chem. Soc.* **2007**, *129*, 10094.
- (10) Kaesz, H. D.; Saillant, R. B. *Chem. Rev.* **1972**, *72*, 213.
- (11) Thyagarajan, S.; Incarvito, C. D.; Rheingold, A. L.; Theopold, K. H. *Chem. Commun.* **2001**, 2198.

- (12) Cui, W.; Wayland, B. B. *J. Am. Chem. Soc.* **2006**, *128*, 10350.
- (13) Konnick, M. M.; Gandhi, B. A.; Guzei, I. A.; Stahl, S. S. *Angew. Chem., Int. Ed.* **2006**, *45*, 2904.
- (14) Wick, D. D.; Goldberg, K. I. *J. Am. Chem. Soc.* **1999**, *121*, 11900.
- (15) Denney, M. C.; Smythe, N. A.; Cetto, K. L.; Kemp, R. A.; Goldberg, K. I. *J. Am. Chem. Soc.* **2006**, *128*, 2508.
- (16) Carmona, D.; Lamata, M. P.; Ferrer, J.; Modrego, J.; Perales, M.; Lahoz, F. J.; Atencio, R.; Oro, L. A. *J. Chem. Soc., Chem. Commun.* **1994**, 575.
- (17) Takahashi, Y.; Hashimoto, M.; Hikichi, S.; Akita, M.; Moro-oka, Y. *Angew. Chem., Int. Ed.* **1999**, *38*, 3074.
- (18) Ahijado, M.; Braun, T.; Noveski, D.; Kocher, N.; Neumann, B.; Stalke, D.; Stammler, H.-G. *Angew. Chem., Int. Ed.* **2005**, *44*, 6947.
- (19) Tejel, C.; Ciriano, M. A.; Jiménez, S.; Passarelli, V.; López, J. A. *Angew. Chem., Int. Ed.* **2008**, *47*, 2093.
- (20) Heidin, Z. M.; Rauchfuss, T. B. *J. Am. Chem. Soc.* **2007**, *129*, 14303.
- (21) Karlin, K. D.; Ghosh, P.; Cruse, R. W.; Farooq, A.; Gultneh, Y.; Jacobson, R. R.; Blackburn, N. J.; Strange, R. W.; Zubieta, J. *J. Am. Chem. Soc.* **1988**, *110*, 6769.
- (22) Heyduk, A. F.; Macintosh, A. M.; Nocera, D. G. *J. Am. Chem. Soc.* **1999**, *121*, 5023.
- (23) Teets, T. S.; Lutterman, D. A.; Nocera, D. G. *Inorg. Chem.* **2010**, *49*, 3035.
- (24) Odom, A. L.; Heyduk, A. F.; Nocera, D. G. *Inorg. Chim. Acta* **2000**, *297*, 330.